Differential Endocytic Functions of *Trypanosoma brucei* Rab5 Isoforms Reveal a Glycosylphosphatidylinositol-specific Endosomal Pathway*

Arun Pal, Belinda S. Hall, Darren N. Nesbeth‡, Helen I. Field§, and Mark C. Field¶

From the Wellcome Trust Laboratories for Molecular Parasitology, Department of Biological Sciences and Centre for Molecular Microbiology and Infection, Imperial College of Science, Technology and Medicine, Exhibition Road, London SW7 2AY, United Kingdom

We demonstrate the presence of a glycosylphosphatidylinositol (GPI) anchor-specific endosomal pathway in the protozoan pathogen *Trypanosoma brucei*. In higher eukaryotes evidence indicates that GPI-anchored proteins are transported in both the endocytic and exocytic systems by mechanisms involving sequestration into specific membrane microdomains and consequently sorting into distinct compartments. This is potentially extremely important in trypanosomatids as the GPI anchor is the predominant mechanism for membrane attachment of surface macromolecules, including the variant surface glycoprotein (VSG). A highly complex developmentally regulated endocytic network, vital for nutrient uptake and evasion of the immune response, exists in *T. brucei*. In common with mammalian cells an early endosomal compartment is defined by Rab5 small GTPases, which control transport processes through the endosomal system. We investigate the function of two trypanosome Rab5 homologues. TbRAB5A and TbRAB5B, which colocalize in the procyclic stage, are distinct in the bloodstream form of the parasite. TbRAB5A endosomes contain VSG and transferrin, endocytosed by the *T. brucei* GPI-anchored transferrin receptor, whereas TbRAB5B endosomes contain the transmembrane protein ISG_{100} but neither VSG nor transferrin. These findings indicate the presence of trypanosome endosomal pathways trafficking proteins through specific routes depending on the mode of membrane attachment. Ectopic expression of mutant TbRAB5A or -5B indicates that TbRAB5A plays a role in LDL endocytosis, whereas TbRAB5B does not, but both have a role in fluid phase endocytosis. Hence TbRAB5A and TbRAB5B have distinct functions in the endosomal system of *T. brucei*. A developmentally regulated GPI-specific endosomal pathway in the bloodstream form suggests that specialized transport of GPI-anchored proteins is required for survival in the mammalian host.

Trypanosoma brucei, a protozoan parasite and the causative agent of African sleeping sickness, evades the immune response primarily by a process of antigenic variation (1). Expression of the major surface antigen, variant surface glycoprotein (VSG),[1] is periodically switched from one gene to another, resulting in the production of a surface with an antigenically distinct VSG and preventing recognition by the host immune system (2). Additional host defense mechanisms include the presence of endogenous lytic factors in the bloodstream (3, 4); trypanocidal activity is mediated at least in part by endocytosis of these factors by the parasite (5). A highly active recycling process is also involved in the trypanosome response to recognition of the surface by host antibody as immunoglobulin bound to surface VSG is capped, endocytosed, and proteolyzed (6). Hence, the endocytic system is an important component of the host-parasite interface.

Unusually, in trypanosomatids all endocytic transport from the plasma membrane is restricted to the flagellar pocket, an invagination of the plasmalemma surrounding the flagellum where it enters the cell body, and is partly isolated from the bulk plasma membrane by desmosomal-like structures. These organisms also use GPI anchors as the predominant mechanism for cell surface attachment of proteins and other macromolecules (7, 8). Several recently characterized proteins also cycle through the *T. brucei* endocytic system including the bloodstream form-specific invariant surface glycoprotein 100 (ISG_{100}) (9, 10) and p67/CB1 (11). Most recently it was reported that endocytosis in bloodstream form involves the presence of a polylactosamine (pNAL)-containing determinant present on a subset of surface glycoproteins and recognized by tomato lectin, but the molecular mechanism underpinning this specificity is not yet clear (12). The presence of glycolipid raft-like structures in both *T. brucei* and *Leishmania major* indicates that lipid-based sorting also operates in these organisms (13).

Endocytosis is under strict developmental control in *T. brucei*. The bloodstream form is highly active in fluid phase and receptor-mediated pathways, with one of the highest rates of membrane turnover recorded. This contrasts with the procyclic pathway where endocytic flux is substantially lower (14) and endocytic activity correlates well with expression of the trypanosome clathrin heavy chain (15). The significance of the high rate of bloodstream form endocytosis is explained in part by a requirement for rapid antibody clearance from the para-

‡ Present address: Guy's, Kings and St. Thomas' School of Medicine, Dept. of Molecular Medicine, Rayne Institute, 123 Coldharbor Lane, London, SE5 9NU, UK.

§ Present address: Proteometrics LLC, P. O. Box 32323, London SW17 8JZ, UK.

¶ To whom correspondence should be addressed. Tel.: 01144-020-7594-5277; E-mail: mfield@ic.ac.uk.

[1] The abbreviations used are: VSG, variant surface glycoprotein; GST, glutathione *S*-transferase; ISG, invariant surface glycoprotein; LY, Lucifer yellow; pNAL, poly-*N*-acetyllactosamine; TES, *N*-tris(hydroxymethyl)methyl-2-aminoethanesulfonic acid-buffered saline; TF, transferrin; GPI, glycosylphosphatidylinositol; PBS, phosphate-buffered saline; BSA, bovine serum albumin; DAPI, 4,6-diamidino-2-phenylindole; WT, wild type; LDL, low density lipoprotein.

site surface (6). *T. brucei* also utilizes the endocytic pathway to acquire nutrients, including low density lipoprotein (LDL), an essential source of lipids, and transferrin, ligands for which the parasite has specific receptor systems. LDL is essential for parasite growth *in vitro* (16), and the system operates in both life stages. Although not defined at the molecular level, both a high (~2 nM) and low affinity binding site (~100 nM) have been described for LDL (17). The transferrin receptor, the product of the *ESAG6* and *ESAG7* genes, is expressed exclusively in the bloodstream form (18).

Rabs are low molecular mass GTPases essential for eukaryote protein trafficking (19). The Rab5 subfamily is essential for the control of traffic through the early endosomal system, and Rab5 compartments interface with recycling systems, controlled in part by Rab4 and Rab11, as well as pathways leading to the lysosome. *In vitro* studies indicate that nucleotide hydrolysis governs the period during which a docking vesicle is fusion-competent (20), whereas Rab5 interacts with a large number of effector molecules, including cytoskeletal proteins, signaling molecules, and components of the soluble *N*-ethylmaleimide-sensitive factor attachment protein receptor vesicle fusion system (21, 22). Expression of dominant negative GDP-bound Rab5 mutants result in decreased endosomal volume, whereas expression of constitutively active GTP-bound Rab5 mutants leads to endosomal swelling and fusion (23). In most systems there are multiple Rab5 isoforms, and genetic analysis in *Saccharomyces cerevisiae* suggests partial redundancy (24). In metazoans evidence indicates nonequivalent functions for Rab5 isoforms based on sensitivity to *Listeria monocytogenes* infection and enhancement of epidermal growth factor receptor endocytosis by some Rab5 isoforms but not others (25, 26).

Two Rab5 homologues have been described in *T. brucei*, TbRAB5A and TbRAB5B (9). The genes are constitutively expressed at the mRNA level, and their protein products localize to vesicular structures in the flagellar pocket region, suggesting involvement in endocytic processes. In addition, homologues of Rab4 and Rab11, TbRAB4 and TbRAB11, are localized to structures in intimate contact with the TbRAB5A compartment and are potentially involved in recycling pathways (9, 27). Here we have investigated the relationship between TbRAB5A and TbRAB5B with cargo molecules and assessed their individual contributions to endocytosis. Our data demonstrate that TbRAB5A and TbRAB5B have distinct functions in *T. brucei* and that TbRAB5A controls a GPI-specific pathway.

EXPERIMENTAL PROCEDURES

Materials—All materials were of analytical grade or higher. Human LDL was from Sigma. Radioisotopes were from Amersham Biosciences. Nucleic acid modification enzymes were variously from Stratagene, New England Biolabs, and MBI Fermentas. Culture media and fetal calf serum were from Sigma or Invitrogen unless indicated otherwise.

Antibodies and Immunochemistry Reagents—Anti-TbRAB proteins were made in house and are described below or in previous publications (9, 28). Anti-VSG (221) rabbit antibodies were made by immunization with soluble VSG following hypotonic lysis of 221 bloodstream forms and DEAE ion exchange purification. Anti-ISG$_{100}$ was the gift of Derek Nolan (Brussels, Belgium). Fluorescent LDL, bovine serum albumin (BSA), Lucifer Yellow, and transferrin were from Molecular Probes.

Trypanosomes—Procyclic culture form *T. brucei*, strain 427, was grown at 27 °C in SDM79 (29) supplemented with 10% heat-inactivated fetal calf serum and 7.5 μg ml^{-1} hemin. Cells were maintained at 5 × 10^5–1 × 10^7 cells ml^{-1} in polystyrene flasks (Corning Glass). 427 bloodstream form cells were cultured as described (27). For quantitation of cell numbers, aliquots of cultures were withdrawn and diluted with 10 ml of Isoton2 medium (Beckman Coulter), and cell number was determined with a Z2 Coulter Counter, averaging at least three measurements. Generation times were calculated using data from replicate cultures followed by regression analysis using Prism (version 2.0a). For

SDS-PAGE analysis freshly harvested trypanosomes were washed in phosphate-buffered saline (PBS) before being added to 2× SDS-PAGE sample buffer and heated to 95 °C for 3 min with occasional vortexing before analysis.

Nucleic Acids and Recombinant DNA Methods—Molecular biology grade water was from an Elgastat Option 4 system (Elga, London, UK). Plasmids were grown in *Escherichia coli* XL1-Blue (Stratagene) or DH5α following transformation by electroporation with a BTX 600 ECM electroporator. PCR products and gel-embedded DNA fragments were purified using Geneclean (Bio 101, Inc.), whereas plasmid DNA was purified using Qiagen kits following the manufacturers' instructions. Small scale plasmid preparations were performed using the Promega Wizard system.

Site-directed Mutagenesis—For mutagenesis of TbRAB5A, the pALTER1 vector (Promega Corp.) was used with the Altered Sites TM system, following the manufacturer's instructions. The TbRAB5A WD-TAGQE motif was mutagenized with an Ala to Thr substitution, and a silent *Pst*I site introduced as a marker for restriction analysis via a second AT substitution. The oligonucleotide was GGGATACTG-CAGGGCTGGAGCGCTACCG. For all other mutants, mutagenesis was carried out by PCR, and assembly was performed in pBlueScript. Site-directed PCR mutagenesis was performed to introduce the Gln to Leu exchange for the GTP-locked TbRAB5B and the Ser to Asn exchange for the GDP-locked form of both TbRAB5A and −5B. Flanking primers included a *Hin*dIII restriction site at the 5′-end and a *Bam*HI site at the 3′-end for subsequent ligations into expression vectors. Primers were designed to amplify open reading frames only. Ser to Asn exchanges created a new *Acs*I site; the Gln to Leu exchange in TbRAB5B created a unique *Xba*I site. Wild type TbRAB5B open reading frame was PCR-amplified from genomic DNA using CTTAAGCTTGTCCATGTCTGT-GAAGACCG and AACGGATCCCAACAACATGCAGTGCTTCAACC. For Ser to Asn exchanges, the AGT at 85–87 bp (TbRAB5A) or TCA at 76–78 bp (TbRAB5B) 3′ to the start codon was replaced by AAT using long primers harboring a *Hin*dIII site and the start ATG at the 5′-end and the exchange at the 3′-end. GDP-locked TbRAB5A^{SN} was PCR-amplified using CTTAAGCTTATGTCGGTGTCAGCGACACCATACA-AACGACAGGATGCAATAACCGCCAGAACTGTTTTGCTCGGGGAG-AGTGCAGTAGGAAAGAATTCC and AACGGATCCCAACAACATGC-AGTGCTTCAACC. GDP-locked TbRAB5B^{SN} was PCR amplified using CTTAAGCTTGTCCATGTCTGTGAAGACCGTTGCCGCCCCCAACAAA-AAAGTACAAAATTGTCCTTTTGGGCGATAGCGGTGTTGGTAAAAA-TTCCC and AACGGATCCCAACAACATGCAGTGCTTCAACC. For TbRAB5B^{QL} the mutagenesis was done by creating two gene fragments with an overlap bearing the mutation and an *Xba*I site. The 5′-fragment bore a *Hin*dIII site, the start ATG, and the mutation, and the 3′-fragment bore the mutation, stop codon, and a *Bam*HI site. 5′-Fragment oligonucleotides for TbRAB5B^{QL} are CTTAAGCTTGTCCATGTCTGT-GAAGACCG and CCAGACTTTTGTAGCGTTCTAGACCGGC, and the 3′-fragment oligonucleotides are CCGGTCTAGAACGCTACAAAA-GTCTGGC and CCGGTCTAGAACGCTACAAAAGTCTGGC. All constructs were verified after assembly by sequence analysis on a 377 PerkinElmer Life Sciences Sequencing system, using Big Dye™ chemistry (PerkinElmer Life Sciences) prior to further analysis. The relevant TbRAB5 open reading frames were subcloned into pXS219 for expression in procyclics or pXS519 for expression in bloodstream forms (derivatives of pXS2 and pXS5 containing the pUC19 polylinker (30).[2]

Electrotransformation of Trypanosomes—For transformation of procyclics, 4 × 10^7 cells of a fresh overnight culture in log phase were centrifuged for 10 min at 800 × *g*, washed in 10 ml of Opti-MEM (Invitrogen), centrifuged again, and finally resuspended in 800 μl of Opti-MEM. These cells were then transferred into 4-mm gap electrocuvettes (Bio-Rad) and mixed with appropriate amounts of vector DNA (typically ~10 μg) for electroporation in an ECM600. The volume in each cuvette was adjusted to 900 μl with Opti-MEM, and samples were chilled on ice prior to electroporation (720-ohm resistance, 2-kV charging voltage, 6.25 kV cm^{-1} desired field strength, and 5-ms desired pulse length). Samples were immediately transferred into 10 ml of nonselective SDM79 immediately after electroporation. Approximately 16 h following electroporation Geneticin (G418) was added to cultures at 65 μg ml^{-1} to select for transformants. Single cell clones were derived as described (30). Bloodstream form trypanosomes were harvested from a 50-ml culture in exponential growth (2 × 10^6 cells/ml) at 800 × *g* for 10 min, washed once in 50 ml of prewarmed cytomix (37 °C), and resuspended in prewarmed cytomix at 8 × 10^7 cells/ml. 450 μl of this suspension was premixed with 10 μg of vector DNA, and pulses were

---

[2] M. C. Field, unpublished data.

administered in 2-mm ice-cold electrocuvettes (Bio-Rad) at 1.5 kV and 25 microfarads in a GenePulser II (Bio-Rad). Cells were then transferred into sterile flasks prepared with 50 ml of HMI9. Cloned cell lines were obtained by serial dilution under antibiotic selection (2.5 μg ml^{-1} G418, Sigma).

PCR—PCR amplification of *T. brucei* total genomic DNA was performed on small scale genomic preparations (31) using 5 ml of dense cultures ($\sim$2 × 10^7 cell ml^{-1}). Each PCR was set up in a 0.5-ml microcentrifuge tube with a total volume of 50 μl. The reaction mixture consisted of 7 mM MgCl$_2$, 250 mM dNTP, $\sim$20 ng of template genomic DNA, 30 pmol each of forward and reverse primers, 2 units of *Taq* DNA polymerase, and 1× reaction buffer. The reactions were performed in a PerkinElmer Life Sciences 480 DNA Thermal Cycler. *Taq* polymerase was added after the reaction was heated to 94 °C for 5 min to denature template DNA (hot start). Thirty cycles were used per reaction, with a 94 °C, 1-min denaturation step, a 58 °C, 1-min annealing step, and extension at 72 °C for 1 min. Primers corresponding to sequences from pXS219 or pXS519 flanking the cloning site were used for detecting integrated copies of the various transgenes. Insertion of the correct mutant or wild type was scored by restriction analysis using the silent sites incorporated during the mutagenesis procedure.

Protein Electrophoresis and Western Blotting—5 × 10^6–2 × 10^7 cells per lane were electrophoresed on 15% SDS-PAGE minigels as described (32) and wet-blotted at 100 V for 3 h in a Transphor Electrophoresis apparatus (Hoeffer Scientific Instruments) in freshly prepared transfer buffer (50 mM Tris, 380 mM glycine, 0.1% (w/v) SDS, and 20% (v/v) methanol) onto 0.45-μm nitrocellulose membrane (Hybond, Amersham Biosciences). After blocking for 1 h in buffer A (PBS with 0.1% (v/v) Tween 20 and 2% (w/v) nonfat dried milk) at room temperature, membranes were washed 3 times in PBS plus 0.1% Tween 20 (PBST) and incubated with primary antibody (diluted 1:1000 in buffer A) for 1 h. After three 5-min washes in PBST the membrane was incubated with horseradish peroxidase-conjugated (Sigma) goat anti-rabbit antisera (diluted 1:20,000 in buffer A) for 1 h followed by four 15-min washes in PBST. Visualization was by enhanced chemiluminescence. Equivalence of loading was ensured by both determination of cell number before sample preparation and Coomassie Blue staining following electrophoresis.

Bacterial Expression and Immunization—The open reading frames for TbRAB5A, TbRAB5A^{QL}, TbRAB5B^{QL}, TbRAB5B^{SN}, and TbRAB5B were expressed from pGEX in *E. coli* as glutathione *S*-transferase (GST) fusion proteins and purified by standard procedures on glutathione-agarose (Amersham Biosciences). All expression constructs were verified by sequence analysis on a 377 PerkinElmer Life Sciences Sequencing system, using Big Dye^{TM} chemistry. Plasmids produced a band of $\sim$50 kDa upon induction for all constructs, the predicted molecular mass for a GST·TbRAB5 fusion protein. Protein was quantitated by SDS-PAGE and Coomassie Blue staining following purification on glutathione-agarose. Antibodies to TbRAB5A and TbRAB5B were prepared by immunization with proteins cleaved from GST beads using factor Xa and raised in a rabbit using MPL^{TM} as adjuvant (Sigma). Preparation of GST·TbRAB2 has been described previously (28). Antibodies were purified from clotted whole serum by affinity chromatography on CNBr-Sepharose immobilized TbRAB5A or TbRAB5B as appropriate. Specificity was monitored by Western blot analysis against the cognate and noncognate TbRAB5 isoform in whole cell *E. coli* lysates. Antibodies only recognized the cognate TbRAB5 (data not shown).

GTPase Assay—Affinity-purified recombinant GST-TbRAB5A, GST-TbRAB5B, GST-TbRAB2, and corresponding QL and SN mutant forms (28) bound to reduced glutathione beads were quantitated by Coomassie Blue staining following SDS-PAGE, and equal amounts ($\sim$10 μg each) were incubated with 10 μCi of [α-^{32}P]GTP in loading buffer (50 mM Tris-HCl, pH 7.5, 50 mM NaCl, 5 mM EDTA, 0.1 mM EGTA, 0.1 mM dithiothreitol, 10 μM ATP) for 10 min at 37 °C. After loading of the radiolabeled nucleotide, the beads were washed three times with ice-cold wash buffer (50 mM Tris-HCl, pH 7.5, 20 mM MgCl$_2$, 1 mM dithiothreitol, 1 mg ml^{-1} BSA) before initiation of hydrolysis by incubation at 37 °C. At each time point an aliquot of the reaction was quenched by adding an equal volume of quench buffer (5 mM EDTA, 50 mM GTP, 50 mM GDP). The degree of hydrolysis was analyzed by separating quenched reactions on 0.1-mm cellulose TLC plates (Macherey-Nagel), with 0.75 M KH$_2$PO$_4$ as mobile phase (33). The TLC plate was air-dried and transferred to a PhosphorImager cassette for detection (Molecular Dynamics Inc.). The ratio of GTP to GDP at time zero was set as 0 percent hydrolysis (note that [α-^{32}P]GTP as supplied by the manufacturer contains trace levels of GDP). Nonenzymatic hydrolysis was monitored by assays that included glutathione beads without recombinant

fusion protein and was typically less than 5% after 2 h of incubation (28).

Lucifer Yellow Uptake—To assay for endocytosis of a fluid phase marker with time, log phase cells were harvested, and appropriate cell numbers (2.5 × 10^7/measurement) were centrifuged (1,200 × *g*, 5 min, 4 °C), resuspended in TES (30 mM TES, 16 mM Na$_2$HPO$_4$, 5 mM KH$_2$PO$_4$, 120 mM NaCl, 5 mM KCl, 3 mM MgSO$_4$, 10 mM glucose, 0.2 mM adenosine, pH 7.5) containing 3 mg ml^{-1} Lucifer Yellow (Molecular Probes), and cultures divided into 3 aliquots for incubation at 27 (procyclic), and 37 (bloodstream form), and 0 °C for specific times before being washed five times with 1 ml of PBS (tabletop centrifuge, top speed, 40 s, 4 °C). The final pellet was resuspended in 100 μl of 1% SDS in TES to lyse cells and release internalized Lucifer Yellow for spectrophotometric assay. 90 μl of each sample was resuspended in 2 ml of 1% SDS/TES in a cuvette for analysis. At each measurement, the fluorescence at 0 °C was subtracted from that obtained at 27 or 37 °C. Fluorescence was quantitated with a Luminescence Spectrometer LS50B (PerkinElmer Life Sciences) configured at λ_{em} 532 nm, λ_{abs} 428 nm, 10 nm slit width. 1% SDS/TES was used as a blank and a range of Lucifer Yellow concentrations used for calibration.

Fluorescence Microscopy—Procyclic trypomastigotes were adhered to precoated poly-L-lysine slides for 3 min at room temperature (Sigma), fixed for 20 min in 4% paraformaldehyde in PBS (Sigma), and permeabilized with 0.1% Triton X-100 in PBS as described (28), and antigen was visualized with fluorescein isothiocyanate, rhodamine, or Cy3-labeled goat anti-rabbit IgG (Sigma). The procedure for fluorescent staining of bloodstream forms was identical, except that the cells were adhered to slides in PBS, 10 mM glucose for 15 min at 4 °C prior to fixation. For accumulation of BODIPY®-conjugated bovine serum albumin, procyclic trypomastigotes were harvested and resuspended in serum-free SDM79 medium containing 1% BSA, incubated for 5 min at 27 °C, pelleted, resuspended in 100 μl of SDM79 containing 2 mg ml^{-1} BODIPY-BSA (Molecular Probes), and incubated for 10 min at 27 °C before fixing as above. For LDL, log phase parental or mutant trypomastigotes were harvested and adhered to poly-L-lysine-coated slides (Sigma) for 3 min. Cells were fixed with 4% paraformaldehyde for 20 min and then washed with PBS (Sigma). For visualization of LDL-binding sites, procyclics were stained with 10 μg/ml BODIPY-LDL (Molecular Probes) in goat serum/PBS for 1 h at room temperature. All slides finally washed with PBS and incubated with 1 mg/ml DAPI (Sigma) for 1 min before final washing with PBS and mounting with Vectastain (Vectalabs). Cells were examined using a Nikon Microphot II microscope and images captured with a Photometrics CH250 Slow Scan charge-coupled device camera. Images were digitized using IP Lab spectrum 3.1 software, false colored, and assembled into figures using Adobe Photoshop 5.0 (Adobe Systems, Inc.).

Preparation of Radiolabeled LDL and Transferrin—LDL quantities are expressed as mass of apoB, the major protein component of LDL. 100 μg of LDL was iodinated with 0.5 mCi of carrier-free Na^{125}I (100 mCi/ml) using chloramine T (Sigma). LDL and chloramine T were separately dissolved in sterile buffer (0.5 M sodium phosphate buffer, pH 7.5) to obtain a 1 and 0.56 mg/ml solution, respectively. 100 μl of LDL solution, 5 μl of Na^{125}I (0.5 mCi), and 60 μl of chloramine T solution were mixed rapidly, and after incubation for 1 min at room temperature, the reaction was quenched with 100 μl of saturated tyrosine. Iodinated LDL was separated from nonincorporated radioactivity and tyrosine on a Sephadex G-25 column (Amersham Biosciences) pre-equilibrated with 25 ml of sterile PBS (Sigma). The ^{125}I-LDL preparation was subjected to TLC and SDS-PAGE to characterize the site of iodination; essentially all radiolabel was found in a chloroform/methanol/water (10:10:3 v/v/v) extract that migrated on silica TLC plates as free lipid species. To prepare cold competitor, a 5 mg/ml stock solution of native LDL in sterile PBS was clarified by passage through a 0.45-mm syringe filter (Nylon Acrocons). Transferrin (TF) was iodinated using chloramine T in a similar fashion and purified by gel filtration through a PD10 column.

LDL Binding and Uptake Assays—Binding studies were performed as described (17, 34) with slight modification. Log phase trypanosomes at a density of $\sim$10^7 cells ml^{-1} were harvested by centrifugation. All subsequent washing and centrifugation steps were performed at 4 °C unless otherwise stated. Cells were pelleted, 10 min, 800 × *g*, washed once with 50 ml of PBS, twice with 10 ml of TES, resuspended in a 5 mg/ml heparin solution in TES to strip off surface-bound LDL, and incubated for 2 h at 4 °C under constant agitation. Cells were spun and washed twice in TES, 1% BSA, and twice in TES alone to remove any heparin and resuspended in TES to a total volume of 0.5 ml. The cell density was determined and normalized for all samples, typically 6 × 10^7 cells ml^{-1}. Cell suspensions were then split into 0.5-ml aliquots in
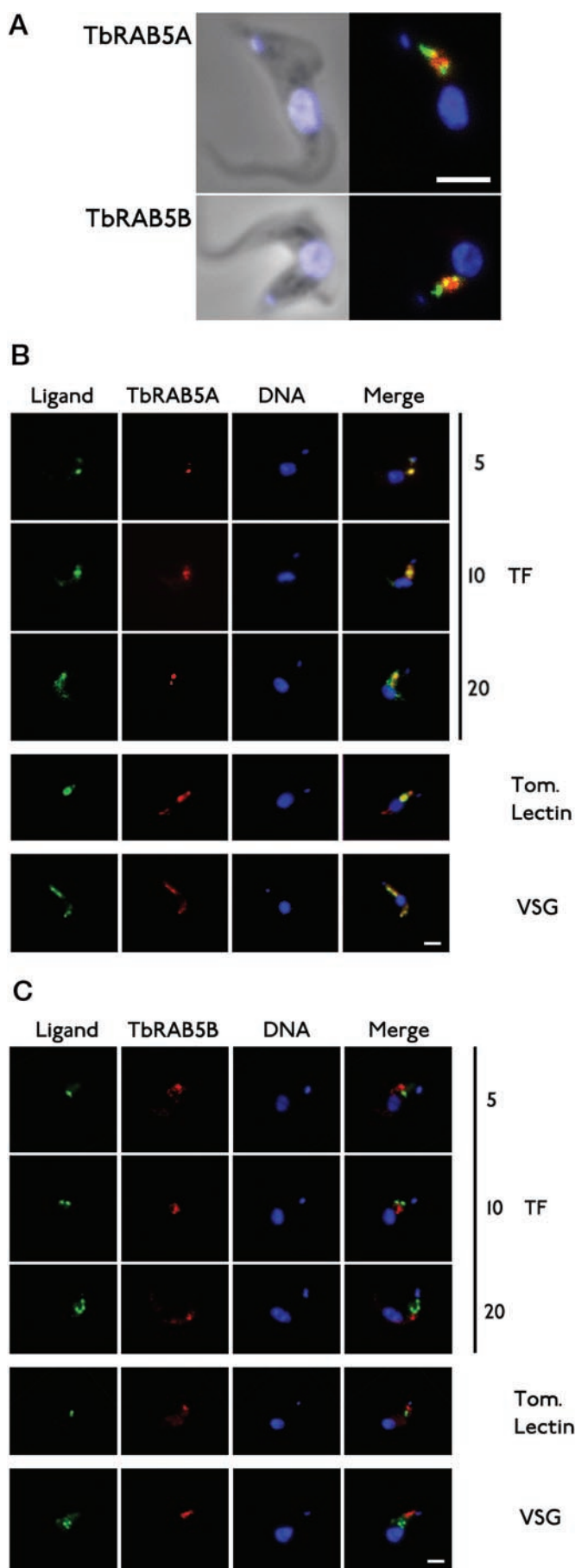
Differential Endocytic Functions of T. brucei Rab5 Isoforms

FIG. 1. **TbRAB5A and TbRAB5B are part of the endocytic system in _T. brucei._** *A*, TbRAB5 compartments are stained with Lucifer

Eppendorf tubes. Native and radiolabeled LDL were premixed in TES, and 0.5-ml aliquots were transferred to the cell suspensions to obtain 1-ml samples of 3×10^7 cells ml^{-1} with 40, 140, 540, 2040, 5040, 20,040, 50,040, and 250,040 ng ml^{-1} final concentrations of total LDL (all in triplicate) and 10^6 ng ml^{-1} (in duplicate). Samples were incubated for 5 h at 4 °C under constant agitation, and cells pelleted for 5 min at $3,000 \times g$ and washed twice in PBS, 0.5% BSA, and cell-associated radioactivity was determined in a gamma counter (Amersham Biosciences). Data were corrected for nonspecific binding as defined by cell-associated radioactivity in the presence of high concentration of native LDL (10^6 ng ml^{-1}). Equilibrium constants (K_d) and receptor numbers per cell were elucidated from a linear plot of [bound/free] *versus* [bound] (Scatchard analysis). For LDL and TF uptake assays, cells were harvested as described for binding studies, washed twice, and resuspended in serum-free medium, 1% BSA, counted, and equalized, typically 2×10^7 cells ml^{-1}. ^{125}I-LDL (320 cpm ng^{-1}) or ^{125}I-TF (7510 cpm ng^{-1}) was added to a final concentration of 120 ng ml^{-1}, and endocytosis was initialized by placing the cell suspension in a water bath at 27 (procylics) or 37 °C (bloodstream form). At suitable time intervals, 0.5-ml aliquots were transferred to Eppendorf tubes on ice prepared with unlabeled LDL or TF to a final concentration of 300 μg ml^{-1} to quench any further uptake and binding. Cells were rapidly pelleted for 1 min at $14,000 \times g$ in a refrigerated centrifuge at 4 °C and supernatants discarded, and cells were washed twice in PBS, 0.5% BSA. Cell-associated radioactivity was determined in a γ-counter (Amersham Biosciences), normalized to 10^7 cells, and converted to cell-associated LDL expressed in mass units (nanograms).

Electron Microscopy—For electron microscopy procyclic cells were grown to log phase and washed in serum-free SDM79 medium prior to fixing with 3% glutaraldehyde and processed for EM as described (35).

RESULTS

TbRAB5A and TbRAB5B Compartments Receive Distinct Endocytic Cargo—We inferred previously (9) that TbRAB5A and TbRAB5B are involved in endocytic transport in *T. brucei* based on the following: (i) positioning in the posterior region of the cell subtending the flagellar pocket; (ii) colocalization of TbRAB5B with ISG$_{100}$, an endosomal protein (10); (iii) close juxtaposition with TbRAB4; and (iv) sequence similarity to mammalian Rab5. We have also shown that TbRAB5A receives fluorescent concanavalin A, which accumulates in this compartment at reduced temperature, strong evidence for a role in endocytosis and probable equivalence with the classical collecting tubules in this organism (27, 36). When procyclic insect form cells were incubated with Lucifer Yellow for 1 h to label extensively the endosomal system, fixed, and stained with antibody to TbRAB5A or TbRAB5B, both TbRAB5A and TbRAB5B structures were partly loaded with Lucifer Yellow, consistent with each being on the endocytic pathway and able to receive fluid phase material (Fig. 1*A*).

To determine whether TbRAB5A and −5B have the same or distinct functions, we compared the cargo that enters these two compartments in bloodstream form, specifically VSG (the ma-

Yellow in bloodstream cells. *Upper panel*, TbRAB5A; *lower panel* TbRAB5B. In each pair of images, phase contrast is to the *left*, and a merged fluorescence image is to the *right. Green*, Lucifer Yellow; *red*, anti-TbRAB5; *blue*, DAPI. *Yellow* stain indicates coincidence of the TbRAB and Lucifer Yellow staining. *B* and *C*, cargo molecules enter the TbRAB5A and TbRAB5B compartments in bloodstream forms. Gallery of images showing various ligands in the TbRAB5A and TbRAB5B compartments in 427 bloodstream cells. *B*, TbRAB5A colocalized with TF, tomato lectin (which binds to polylactosamine glycans), and VSG. In all cases TbRAB5A is in *red*, the second marker in *green*, and DNA in *blue*, with a merged image in the *rightmost panel*. For TF, a time course of accumulation is shown, indicating that TF rapidly enters the TbRAB5A compartment, consistent with assignment as an early endosome. *C*, TbRAB5B colocalized with TF, tomato lectin, and VSG. In all cases TbRAB5B is in *red*, the second marker in *green*, and DNA in *blue*, with a merged image in the *rightmost panel*. Note that VSG and tomato lectin do not colocalize with TbRAB5B, differentiating this compartment from TbRBA5A. For TF, a time course of accumulation is shown, indicating that TF never enters the TbRAB5B compartment. *Scale bars*, 2 μm.
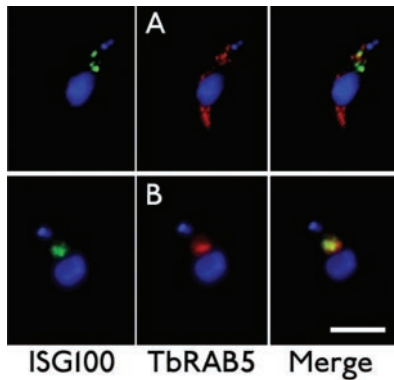
FIG. 2. **Distinct cargoes are present in TbRAB5A and TbRAB5B compartments in bloodstream stage cells.** Immunofluorescence analysis of TbRAB5 compartments in bloodstream *T. brucei*. *Upper panels*, TbRAB5A; *lower panels*, TbRAB5B. In each case ISG$_{100}$ immunofluorescence is shown in *green*, TbRAB5A/B in *red*, and DNA in *blue*. *Rightmost panels* is a merged image; *yellow* stain indicates coincident location for TbRAB5B and ISG$_{100}$. The presence of ISG$_{100}$ in the TbRAB5B compartment of bloodstream form has been reported previously, together with data indicating coincident localization of TbRAb5A and TbRAB5B in procyclics (9). *Scale bars*, 2 μm.

jor surface glycoprotein and GPI-anchored), transferrin (endocytosed by the ESAG6/7 GPI-anchored heterodimer), and ISG$_{100}$ (a transmembrane protein). TbRAB5A extensively colocalized with VSG and transferrin but not with ISG$_{100}$. Significantly, ISG$_{100}$ was found in TbRAB5B-positive structures, whereas this compartment did not contain VSG or transferrin (Fig. 1, *B* and *C*, and Fig. 2). In addition, we observed that the TbRAB5A endosome population in bloodstream forms contained the major proportion of the tomato lectin reactivity (pNAL glycans) associated with endosomal glycoproteins (12). Hence, TbRAB5A and −5B are part of distinct endocytic pathways in the bloodstream form, and in particular, TbRAB5A structures contain GPI-anchored proteins and ligands of GPI-anchored receptors. Because VSG is by far the most abundant surface molecule, these data indicate that the vast majority of GPI-anchored proteins enter the TbRAB5A compartment and are selectively excluded from TbRAB5B endosomes. By contrast, as previously reported (9), both TbRAB5A and TbRAB5B are present on the same membrane structures in procyclics. Overall, these data provide strong evidence that TbRAB5A and TbRAB5B are indeed components of the endocytic machinery, that their relationship is developmentally regulated, and that they have clear and distinct functions.

Production of Mutant TbRAB5 Proteins—To investigate further the functions of TbRAB5A and −5B, we constructed mutant versions of each protein by single amino acid substitution in critical catalytic regions of the proteins. Construction of constitutively GTP-bound Rab5 mutants by QL substitution within the WDTAGQE hydrolytic motif, conserved in the majority of Rab proteins, has been highly successful in determining the functions of Rab5 isoforms in higher eukaryotes and resulting in gain of function activity (23, 24). By contrast, dominant negative forms, produced by an SN mutation in the GKS consensus sequence, bind only GDP. Rab5^{QL} causes enlarged endosomes and perturbation of endocytosis, whereas Rab5^{SN} generates shrunken endosomes (26). The WDTAGQE QL and GKS SN mutants were made for both TbRAB5 proteins.

Given the degree of phylogenetic divergence of TbRAB5 from mammalian Rab5, we wished to demonstrate directly that the Gln to Leu mutants have depleted GTPase activity. Mutant and wild type TbRAB5 proteins, together with TbRAB2 as a control (28), were expressed as GST fusion proteins in *E. coli*,

TABLE I
Analysis of enzymatic function of TbRAB5A, TbRAB5B, and QL isoforms in vitro

All assays were performed in duplicate, using freshly isolated GST fusion proteins coupled to glutathione-agarose (see "Experimental Procedures"). Approximately 10 μg of each protein was used for each reaction and quantitated by Coomassie staining of SDS-PAGE separated protein. Following hydrolysis, products were resolved by TLC. At least five time points were taken for each assay; for brevity and clarity a representative time point within the linear portion of the curve is shown here (typically before 70% of the GTP has been hydrolyzed). Data from a single experiment are shown; all assays were performed at least twice with highly reproducible results. In all cases, the QL mutant had less than 20% of the activity of the corresponding wild type protein. Note that the SN mutants were not assayed due to instability in *E. coli*.

TbRAB	Reaction time	% GTP hydrolysis ($\pm$S.D.)	% TbRAB2 activity
	min		
Assay 1			
2	30	68.8 (1.7)	100
5A	30	42.6 (1.8)	62
Assay 2			
5A	30	46.6 (3.4)	ND[a]
5A^{QL}	30	9.1 (1.2)	ND
Assay 3			
2	40	22.0 (3.7)	100
5B	40	34.1 (3.0)	155
5B^{QL}	40	5.8 (4.5)	26

[a] ND, not determined.

bound to glutathione-Sepharose beads, and their GTPase activity was determined over a 1-h period (Table I). Product production attained a plateau after hydrolysis of >70% of the GTP (28). TbRAB5A and TbRAB5B had hydrolytic activity that was similar to TbRAB2, whereas for both TbRAB5 proteins the Gln to Leu substitution resulted in a significant decrease in GTP hydrolytic activity, with the QL mutants retaining less than 20% of the activity of the corresponding wild type protein (Table I and data not shown). The TbRAB5A^{SN} and TbRAB5B^{SN} proteins were unstable in *E. coli*, which has been observed for several TbRAB^{SN} mutants,[3] and their *in vitro* biochemical properties were not investigated further.

Generation of Procyclic and Bloodstream Form Cell Lines Overexpressing TbRAB5 Isoforms—A total of 12 distinct transgenic constructs were generated, corresponding to wild type, QL, and SN versions of each of the two *TbRAB5* genes and both life stages. 427 strain procyclic or bloodstream form trypanosomes were transfected with TbRAB5A, TbRAB5B, and mutant forms as complete open reading frames in pXS219 or pXS519, respectively, selected, and cloned by limiting dilution (28). Multiple clones were obtained for each construct. To demonstrate the presence of the integrated vector, genomic DNA of parental and transformed cells was extracted for PCR analysis (31). Products of the expected size were recovered from the genome of transfected cells by using vector-specific primers, whereas the parental strain yielded no detectable product, consistent with stable integration of the construct and specificity of the PCR (data not shown). The presence of noncoding restriction markers engineered into the QL and SN substitutions was used to confirm that the correct variant was present (see "Experimental Procedures" and data not shown). These data demonstrated integration of the transgene construct.

Expression of ectopic TbRAB5 at the protein level was determined by Western blot and probing lysates with affinity-purified polyclonal antibodies raised against either recombinant TbRAB5A or −5B (9). In the cell lines expressing ectopic wild type or QL version of the protein, we observed a 4–10-fold increase in signal in the relevant band, consistent with expression of the correct product at increased levels (Fig. 3). For SN

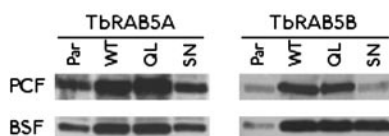[3] M. C. Field and T. Jeffries, unpublished data.

FIG. 3. **Characterization of trypanosome clones overexpressing TbRAB5A or −5B.** Expression of TbRAB5A and −5B in transformed *T. brucei* cells cloned by limiting dilution were analyzed by Western blot. Boiling SDS lysates of trypanosome cells (typically 5 × 10^6 per lane) were prepared, fractionated by reducing SDS-PAGE, probed with rabbit anti-TbRAB5A or −5B polyclonal antibodies, and raised against recombinant protein expressed in *E. coli* as indicated. Equivalence of loading was determined by Coomassie Blue staining of aliquots of the lysates electrophoresed on identical gels. Note that the anti-TbRAB5 antisera are monospecific as determined by Western analysis of the affinity-purified antibodies when used to probe *E. coli* lysates containing GST-TbRAB5A or −5B (data not shown). *Par*, parental; *PCF*, procyclic; *BCF*, bloodstream.

TABLE II
Overexpression of TbRAB5A, TbRAB5B, and mutant isoforms results in altered growth in procyclic form T. brucei

Cells were inoculated into fresh media at 10^5 parasites/ml. Growth was followed over a period of at least 5 days, determining cell number twice daily with a Coulter counter. Regression analysis was used to determine the generation time. All experiments were carried out in at least duplicate experiments (*n*, number of experiments). Growth phenotype has been observed to be stable over a period in excess of 100 generations. For bloodstream mutants the deviation from parental growth was not statistically significant.

	Generation time	Percent (parental = 100)	*n*
	h		
Procyclic			
Parental	16.9 ± 0.3	100	3
5AWT	22.8 ± 0.1	135	2
5AQL	15.1 ± 1.1	89	2
5BWT	23.1 ± 2.0	137	6
5BQL	23.3 ± 2.2	138	4
Bloodstream form			
Parental	9.2 ± 0.1	100	2
5AWT	9.9 ± 1.0	107	2
5AQL	9.1 ± 0.1	99	2
5BWT	9.2 ± 0.6	100	2
5BQL	10.5 ± 1.2	115	2
5BSN	10.4 ± 1.0	114	2

forms expression was lower, and by this analysis only the TbRAB5BSN form in the bloodstream form could be positively detected, and hence the SN mutants may be less stable *in vivo* than QL or WT forms, similar to the reduced stability observed in *E. coli*. Moderate expression, as obtained here, of ectopic Rab is preferable as the mutant proteins have dominant effects, and in particular the GTP-locked QL form is generally considered to sequester GTPase activating protein effectors; low expression reduces the possibility of erroneous cross-talk between downstream signaling pathway components.

Characterization of the TbRAB5 Mutant Cell Lines—We initially assessed the influence of the ectopic copy of TbRAB5A, −5B, and the various mutants on growth of *T. brucei* in culture. First, all transformants had normal morphology and unaltered DNA content, indicating normal progression through the cell cycle. Second, growth curves were obtained over a period of 5–7 days and generation times calculated by regression analysis. The data indicate no significant alteration in the growth of bloodstream form cells *in vitro* (Table II), and when used to infect mice, there was also no discernible difference in replication rate.[4] By contrast, overexpression of wild type and QL TbRAB5B isoforms and the TbRAB5AWT in the procyclics resulted in an ~30% decrease in the growth rate. This may be
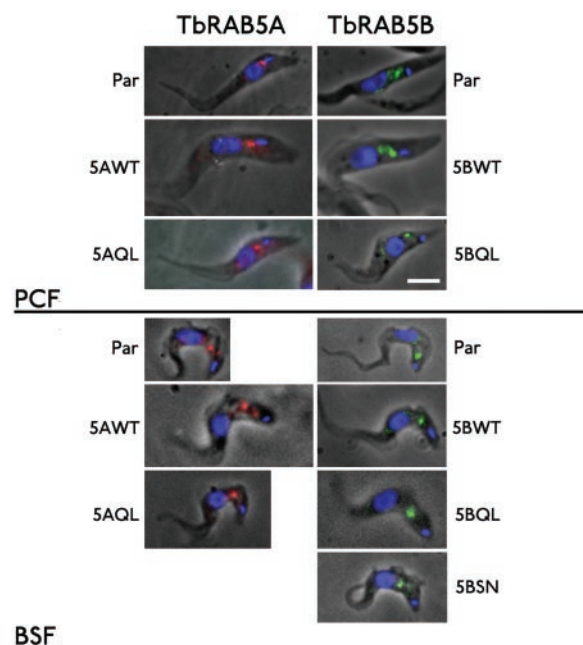
[4] A. Pal, M. C. Field, and H. P. Voorheis, unpublished data.

FIG. 4. **Overexpression of TbRAB5A proteins does not lead to mislocalization.** Gallery of immunofluorescence images of bloodstream and procyclic form parasites showing the location of TbRAB5A and TbRAB5B in parental (*Par*) and cloned transgenic lines. In all panels the TbRAB protein is observed localized to structures between the nucleus and kinetoplast as predicted for an endosomal component and consistent with correct targeting. The life stage (*BSF*, bloodstream; *PCF*, procyclic), cell line, and antiserum used are indicated. Panels show a merge of the phase contrast, DAPI stain for the nucleus and kinetoplast (*blue*), and the fluorescent antibody channel (*FITC*). Note that the images have been false colored for immunoreactivity in *red* (*TbRAB5A*) and *green* (*TbRAB5B*). *Scale bars,* 2 μm.
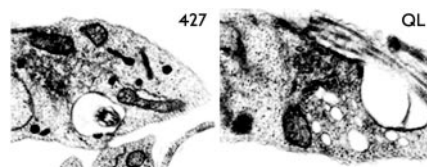

FIG. 5. **Endosomal ultrastructural morphology is perturbed in TbRAB5A^{QL} procyclic cells.** Ultrastructural analysis of mutant and wild type cells by thin section of plastic-embedded cells. *A,* 427 wild type procyclic showing the endosomal region of the trypanosome in the posterior of the cell. *B,* TbRAB5A^{QL} procyclic, showing the same region of the cell as in *A*. Large membrane-bound structures proximal to the flagellar pocket can be clearly observed. Other parts of cytosol are devoid of these structures, indicating a specific effect on this portion of the cell. Magnification factor 25,000× (*A*) and 40,000× (*B*). Other cell lines had no ultrastructural abnormalities (data not shown). *Scale bars*, 0.2 μm.

due to abnormalities in the endosomal system and, in particular, in uptake of vital nutrients. As other parameters indicate that these cells are functioning normally and the growth rate alterations are minor, we conclude that the mutants are unlikely to have major pleiotrophic effects.

Third, to ensure that any phenotype of transgenic parasites was representative of the true functions of TbRAB5A and TbRAB5B, we determined the intracellular localization of the TbRAB5 proteins by immunofluorescence. In no case did we observe aberrant localization; TbRAB5 immunoreactivity was always located to vesicular structures positioned between the nucleus and kinetoplast (Fig. 4), consistent with correct targeting of the TbRAB5A and TbRAB5B proteins (9). By epifluorescence microscopy, alterations to the morphology of the compartments themselves cannot be resolved (see below). Hence, there is no gross alteration to cell cycle, detrimental effects on growth

FIG. 7. **Procyclic trypanosomes expressing TbRAB5A**^{QL} **have augmented LDL endocytosis.** Cells in exponential growth were harvested, washed, and resuspended in TES. Radiolabeled ^{125}I-LDL or TF was added, and after 1 h incubation aliquots were transferred to ice, quenched, and washed extensively as described under "Experimental Procedures." Cell-associated radioactivity was determined in a γ-counter and converted to cell-associated LDL expressed as percent uptake relative to bloodstream cells. Data are the mean of three determinations, and *error bars* indicate the S.D. Background levels of binding, obtained in the presence of excess ligand, have been subtracted from each data point. *Dotted line* indicates the mean level of uptake in bloodstream forms, and all data are normalized to this value at 100%. *Open bar,* parental 427; *gray bar*, TbRAB5B mutants; *dark bar*, TbRAB5A mutants. *PCF*, procyclic; *BCF*, bloodstream.

FIG. 6. **TbRAB5A and TbRAB5B control fluid phase endocytosis.** *A*, specific LY uptake on procyclic (*PCF*) and bloodstream (*BCF*) stage TbRAB5 overexpressors. Cells were harvested from cultures in exponential growth, washed, and resuspended in TES buffer supplemented with 3 mg/ml LY at 2×10^7 cells/ml. Uptake was allowed for 2 h at 30 (bloodstream) or 27 °C (procyclic). Cells were washed five times in TES, lysed in TES, 1% SDS, and cell-associated LY was determined in a fluorimeter. Values were corrected for cell-associated LY obtained over the same time course on ice to express specific uptake. Samples were set up in triplicate. Displayed is the specific LY uptake as fraction (in %) of the bloodstream parental cells, and *error bars* show the difference of two independent experiments. The mean specific LY uptake of bloodstream parental WT cells was 4.67 ± 1.96 ng/10^7 cells, $n = 8$. *Open bar*, procyclic parental; *dark bars*, TbRAB5A isoforms; *light gray bars*, TbRAB5B isoforms. *Dotted line* represents 100% of bloodstream form parental level. *B*, cell-associated fluorescence is shown for a time course of Lucifer Yellow accumulation up to 180 min. The experiment was done in triplicate, with background values obtained from parallel samples maintained on ice before solubilization. Standard error bars are indicated, and this is a representative experiment of two. A clear increase in uptake of Lucifer Yellow is obtained with the TbRAB5A^{WT} overexpressor, which is augmented further for TbRAB5A^{QL}. *Error bars* for some data points are occluded by the plot symbol.

rate, or mistargeting of the G proteins, suggesting that transgenic phenotypes will be ascribable to a specific function of TbRAB5.
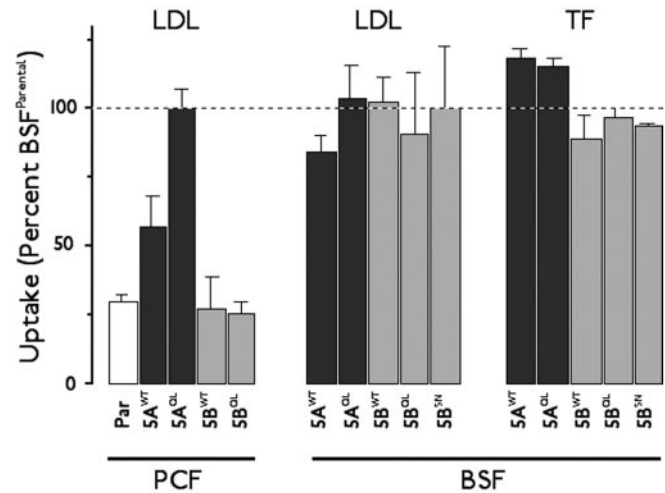
Overexpression of TbRAB5A^{QL} *Increases Endosome Volume*—To investigate the effects of TbRAB5 isoform expression on membrane organization at the ultrastructural level, sections were prepared from silicone-embedded samples of each of the six procyclic transfected strains and the parental cells. In all strains, except the TbRAB5A^{QL} and TbRAB5A^{WT} cells, endosome structure was unaltered. By contrast, in the TbRAB5A^{QL} cells, structures several times larger than normal early endosomes, were observed proximal to the flagellar pocket (Fig. 5). Similar, but less pronounced alterations were visible in the TbRAB5A^{WT} cells (data not shown). The mutant cells exhibited no other abnormal morphology. These enlarged structures possess continuous membranes, suggestive of early endosomes, and were frequently in close contact with each other, which could indicate high levels of homotypic fusion.

TbRAB5A Affects Fluid Phase Endocytosis—Previous studies of trypanosomal endocytosis used fluorescent dextrans as fluid phase markers (5). We chose Lucifer Yellow (LY) to follow endocytosis and recycling by fluorescence spectrophotometry as this compound colocalizes with TbRAB5A and −5B (Fig. 1). We initially screened our panel of mutants for LY uptake over a 2-h period (Fig. 6*A*). Internalization by parental nontransfected procyclic cells was extremely low and just detectable, consistent with previous studies (37), but significantly greater in parental bloodstream forms. Expression of mutant TbRAB5 isoforms had no effect on LY uptake in the bloodstream form, similarly to the lack of enhancement seen with LDL (below). By contrast, LY endocytosis was augmented significantly in the procyclic pathway by the QL isoforms of both TbRAB5A and TbRAB5B, indicating a role in fluid phase endocytosis for both proteins. Significantly, the TbRAB^{QL} mutant augmented LY uptake to a level equivalent to the parental bloodstream form, similar to the data for LDL endocytosis and consistent with the presence of a rate-determining step in bloodstream form endocytosis that cannot be stimulated by TbRAB5. The stimulation by TbRAB5B^{QL} was less marked than TbRAB5A^{QL}, and the
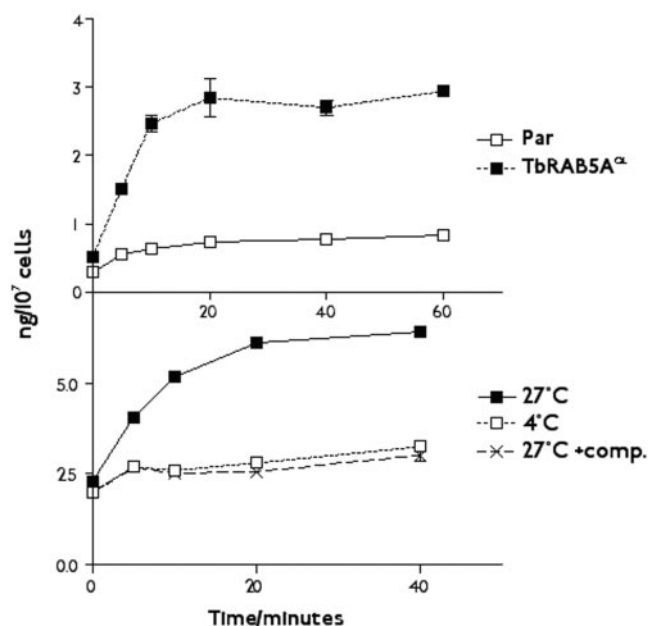
FIG. 8. **Kinetics of LDL uptake are altered in TbRAB5A^{QL} cells.** Time course of LDL accumulation for both parental 427 procyclic cells (*open symbols*) and TbRAB5A^{QL} overexpressors (*closed symbols*). *Error bars* indicate the S.E. from a triplicate determination. *Lower panel*, uptake at 27 °C represents specific uptake of human LDL. Procyclics overexpressing TbRAB5A^{QL} were processed as for the kinetic experiment, and cells were incubated as follows: 27 °C (*closed square*); 27 °C plus 300 μg/ml unlabeled LDL (*cross*); 4 °C (*open square*). Increased binding at $t = 0$ in the *lower panel*; this is due to proportionately greater background from interaction with the plasticware as lower numbers of cells were used in this experiment compared with that shown in the *top panel*. *Par*, parental.

TbRAB5B^{WT} form did not stimulate LY uptake, suggesting a less important role for TbRAB5B than TbRAb5A in procyclic fluid phase endocytosis.

We chose to analyze LY uptake kinetics in TbRAB5A isoform-expressing cells, as TbRAB5A had a more pronounced influence on this parameter (Fig. 6*B*). Compared with the parental line, the TbRAB5A^{QL} clone internalized at over 10-fold more fluorophore in a given period. Significantly, the TbRAB5A^{WT} cells had an intermediate level of endocytosis compared with the parent strain and the TbRAB5A^{QL} cells. As the expression levels of the ectopic TbRAB5A isoforms are very similar, these data indicate that the nucleotide status of TbRAB5A is important in control of endocytosis, whereas comparison between parental cells and the TbRAB5A^{WT} cells indicates that copy number is also a parameter controlling endocytic flux.

GTP-binding State of TbRAB5A Affects Receptor-mediated Endocytic Flux—To analyze the role of TbRAB5A and −5B in receptor-mediated endocytosis, we chose the LDL and the TF receptors (ESAG6/7) for study. LDL and TF are essential requirements for parasite growth (16, 38, 39). The LDL receptor is expressed in both bloodstream form and procyclic stages (17, 38) but has not been cloned, whereas the TF receptor is bloodstream form-specific and well characterized at the molecular level (39).

We screened all procyclic and bloodstream form cell lines for their ability to endocytose LDL and bloodstream form cell lines for TF accumulation during a simple 1-h incubation (Fig. 7). Cells were exposed to ^{125}I-labeled ligand, extensively washed following the incubation, and cell-associated radioactivity determined in a γ-counter. Control experiments demonstrated that for both ligands no uptake was observed in the presence of >100-fold excess unlabeled ligand or at 4 °C and that TF up-

take could be prevented by calcium chelation (data not shown).

For TF, none of the mutant TbRAB proteins altered accumulation, despite data indicating that this ligand is present in the TbRAB5A compartment (Fig. 7). By contrast LDL accumulation was augmented in the procyclic cells expressing the TbRAB5A^{QL} ~5-fold (Fig. 7), resulting in a similar level of LDL accumulation as in bloodstream form cells. None of the bloodstream form mutants or the TbRAB5B procyclic mutants exhibited altered LDL uptake. These data suggest that TbRAB5A has a specific role in LDL endocytosis in the insect stage parasite. The insensitivity of endocytosis to TbRAB5 perturbation in the bloodstream form is unknown but may be connected with the much higher endogenous levels in this stage; in the procyclic TbRAB5A^{QL}, LDL accumulation was increased to levels equivalent to bloodstream form, consistent with the presence of a further rate-limiting process in this stage.

Next we determined the kinetics of LDL accumulation by the procyclic parental and TbRAB5A mutant cell lines. Procyclics take up LDL but at a low level (Fig. 8). The accumulation of LDL attained a plateau after ~30 min due to LDL reaching the lysosome where it is degraded and radiolabel released. Similar uptake was observed for the TbRAB5A^{QL} cells with the exception that the level of LDL accumulated was greatly increased (Fig. 8). No uptake was observed in the presence of excess unlabeled LDL or at 4 °C (Fig. 8). These data indicate that the rate of receptor-mediated endocytosis may be stimulated by TbRAB5A at the insect stage, confirming this Rab protein as a central control element in selected endocytic processes in *T. brucei*.

With the above indication that TbRAB5A, but not TbRAB5B, influences LDL endocytosis, we next asked if receptor location was being altered. Perturbation of endocytic compartments can lead to redistribution of transferrin receptors in metazoan cells (23). As the LDL receptor has not been cloned, we chose to determine the number of LDL-binding sites at the surface of cells at 4 °C. We observed two affinity classes for LDL binding, a high affinity class (K_d 4 nM) and a lower affinity class (K_d 70 nM) by Scatchard analysis using ^{125}I-labeled LDL on the parental procyclic (Fig. 9 and Table III) in agreement with previous observations (17). Scatchard analysis on the TbRAB5A^{WT} and TbRAB5A^{QL} cells identified two sites with essentially identical affinities to the parental line. However, the number of sites was increased ~12-fold in the TbRAB5A^{QL} and 3-fold in the TbRAB5A^{WT} overexpressor cell line (Fig. 9 and Table III). Most significantly, the ratio of the high to low affinity class site was maintained (Table III). We were unable to determine the total level of expression of the LDL receptor as the protein has not been identified and binding studies on whole cell extracts were uninformative, and hence we cannot formally rule out augmented expression of the LDL receptor protein, although we consider this as extremely unlikely.

LDL-binding sites are reported to be located on the flagellar pocket, the flagellar body, and in endosomal structures (17). We examined the location of the LDL receptor in procyclic parental and TbRAB5A^{QL} cells using BODIPY-LDL. This analysis confirmed that most LDL receptors were located on the flagellum and in the flagellar pocket, but importantly that staining intensity was greatly increased in the TbRAB5A^{QL} cells, consistent with a greater LDL receptor number at the cell surface but otherwise unperturbed localization (Fig. 10). The BODIPY-LDL surface staining is not an artifact of the fixation process, because the same pattern was observed by incubating parasites with the fluorescent LDL at 4 °C, prior to fixation (not shown). Together these data indicate that expression of TbRAB5A^{QL} increases the number of surface LDL-binding sites, and the most probable mechanism is that internal receptors are redistributed to the surface by perturbation of endocytic and recy-

FIG. 9. **Scatchard analysis of procyclic form trypanosomes reveals increased surface LDL-binding sites in TbRAB5A mutant cells.** Parental (*Par*) 427 and cells expressing TbRAB5A^{WT} and TbRAB5A^{QL} ectopic copies were analyzed for surface LDL-binding sites by competition binding analysis. Data are presented as [bound/free] against [bound]. All determinations were done in triplicate, with S.E. indicated and have been background corrected. In all cases two affinity binding sites for LDL can be detected but in proportionally greater numbers for TbRAB5A^{WT} and TbRAB5^{QL} compared with the parental cells. *Lines* through the plot symbols represent the regression fit of the data. Note the changes in the scale on the *abscissa*.
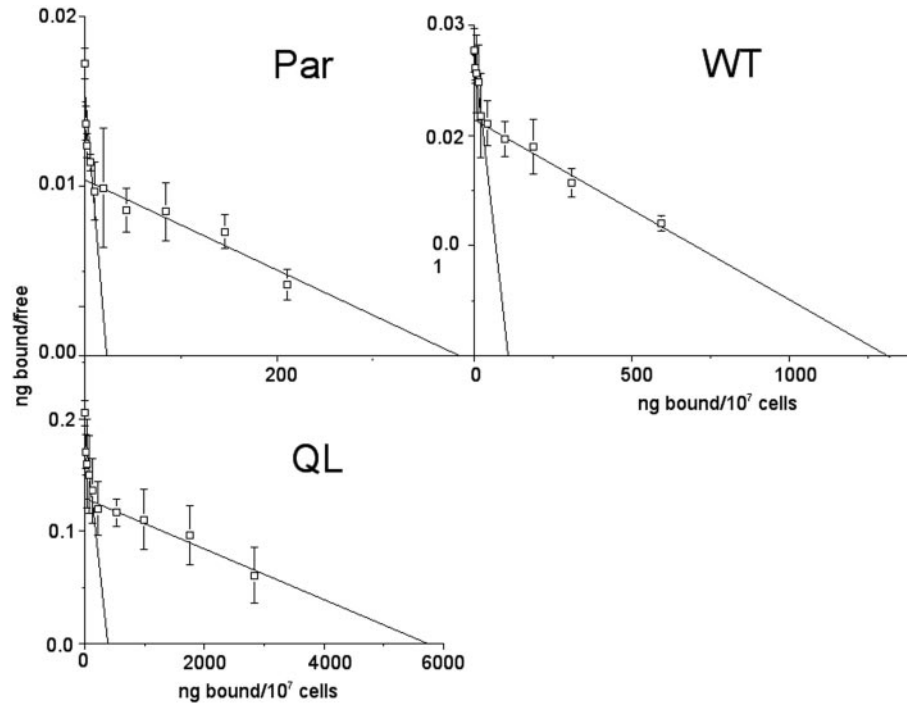
TABLE III
The number of specific LDL-binding sites are increased in the TbRAB5A^{WT} (5A^{WT}) and TbRAB5A^{QL} (5A^{QL}) procyclic overexpressors

Data are derived from Scatchard plots (Fig. 9). The number of specific LDL-binding sites are expressed on a per cell basis. The analysis has been done three times with essentially identical results. Par, parental.

Cell line	Low		High		Ratio[b]
	K_D	Number[a]	K_D	Number	
	nM		nM		
Par[c]	69	43,000	4.1	2,600	0.06
5A^{WT}	111	144,000	7.4	12,100	0.08
5A^{QL}	81	633,000	5.9	44,000	0.07

[a] Number of binding sites/cell in high or low affinity class.
[b] Ratio of the number of high to low affinity binding sites.
[c] 427 is the unmanipulated parental strain for all PCF lines.

cling kinetics. The effects of TbRAB5A^{QL} on LDL uptake in procyclics and the specific trafficking of GPI-anchored proteins through the TbRAB5A compartment also suggest that the parasite receptor for LDL may be a novel GPI-anchored protein.

DISCUSSION

For endocytosis of plasma membrane proteins the route taken is influenced by the mode of membrane attachment, specifically GPI anchor or transmembrane polypeptide. Both cargo classes meet at some point past the early endosome (as defined by Rab5 localization), but controversy remains concerning the relationship of GPI-anchored proteins and the clathrin-dependent endocytic system. In trypanosomatid parasites, endocytosis of GPI-anchored macromolecules is of particular importance as this is the major mechanism for surface membrane attachment, and many of these GPI-anchored molecules are implicated in virulence systems (7). The major functions of the *T. brucei* endocytic system, composed of a set of tubules and vesicles interacting with the flagellar pocket and the *trans*-Golgi network, are nutrient uptake and defense from the humoral arm of the host immune response (15, 40). We and others (9, 10, 14, 15, 27) have mapped an increasing number of compartments responsible for fluid phase and receptor-mediated uptake, part of which is likely to be clathrin-dependent. The TbRAB5 isoforms in the trypanosome have evolved independent of higher eukaryotes, suggesting adaptation to the specific requirements of the parasite (9). The system also contains

recycling endosomes defined by TbRAB4 and TbRAB11 (9, 27).

Metazoan Rab5 isoforms have distinct functions in endocytosis of surface receptors and interaction with intracellular pathogens (25, 26). A revised organization for the endosomal system suggests that endosomal compartments are multifunctional, with Rab5 domains receiving cargo and contiguous but distinct Rab4 and Rab11 domains for recycling (41). We find that in bloodstream form trypanosomes TbRAB5A- and TbRAB5B-positive endosomes contain distinct cargo sets; specifically, the GPI-anchored VSG and transferrin (endocytosed by a GPI-anchored receptor) are present within the TbRAB5A population, whereas transmembrane ISG$_{100}$ localizes to the TbRAB5B compartment and contrasts to the insect form where the two TbRAB5 proteins are coincident (9). These observations suggest that in the bloodstream form there is a requirement for multiple endosomal pathways, *i.e.* a TbRAB5A-dependent endocytic sorting pathway devoted to GPI-anchored proteins and fully separated from a second path mediated by TbRAB5B.

Hence, endocytic sorting of GPI-linked molecules in trypanosomes occurs early and possibly depends on the mechanism of membrane attachment. This hypothesis is supported by data from a study in *Trypanosoma vivax*, where a 65-kDa transmembrane protein was shown to internalize to compartments distinct from VSG following binding of cognate antibody (42). Also, VSG and ESAG6/7 are only distantly related at the sequence level, and any peptidic polypeptide signal is unlikely to
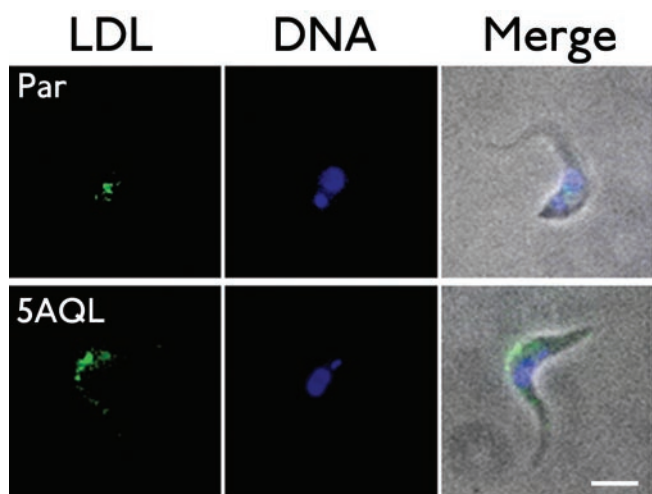
FIG. 10. **Enhanced binding of LDL to the surface of procyclic cells expressing TbRAB5A^{QL} at the flagellar pocket and flagellum.** Parental (*Par*) 427 (*top panels*) and TbRAB5A^{QL} (QL; *bottom panels*) procyclics, fixed and stained with BODIPY-LDL (10 μg/ml) (*left panels*). Nuclei and kinetoplasts were visualized by DAPI staining (*middle panels*). *Right- hand panels*, merge. In the parental the majority of the LDL is bound to the flagellar pocket region, whereas in the TbRAB5A^{QL} cell surface staining is more extensive and extends along the flagellum. Note that these cells have not been permeabilized, so that internal LDL-binding sites are not revealed. *Scale bars*, 2 μm.

be extensive. In *T. brucei* the GPI anchor has been implicated in anteriograde transport, and the presence of glycolipid rafts would be consistent with a GPI-based sorting mechanism (13, 43). Alternatively, pNAL determinants present on several trypanosome proteins may provide a selective endocytic sorting signal, but because VSG does not have tomato lectin-reactive pNAL chains, endocytosis and sorting of this major protein are pNAL-independent, despite being localized to the same compartment as tomato lectin-reactive carbohydrate (12).

These observations and the developmentally regulated VSG recycling TbRAB11 pathway (27) suggests the presence of a specialized pathway for GPI-anchored cell surface proteins probably via TbRAB5A and TbRAB11 compartments. This system may strengthen rapid uptake and recycling of antibody cross-linked VSG (6) and would represent a major mechanism for evasion of the host immune system. In the procyclic this pathway is presumably not required as defense against the less sophisticated insect adaptive immune response seems to be dependent on the ability of the procyclics to prevent access of proteases to the plasma membrane (44).

In our efforts to understand TbRAB5A and TbRAB5B function, we generated cell lines expressing wild type, QL, and SN variants of TbRAB5A and TbRAB5B. We could not overexpress SN forms, most likely due to instability of the protein, but for wild type and QL forms moderate expression was achieved. Overexpression did not result in grossly altered endosomes, mislocalization, alteration to cell cycle behavior, or major changes in generation time, although limited endosomal swelling with TbRAB5A^{QL} was observed. We were unable to detect significant changes in endocytosis in bloodstream parasites but did see significant alterations in insect stage parasites. Specifically TbRAB5A is implicated in LDL endocytosis, and both TbRAB5A and TbRAB5B are involved in fluid phase uptake. The stronger influence of TbRAB5A on endocytosis is consistent with enlargement of endosomal structures, whereas similar alterations were not detectable for TbRAB5B mutants. Of particular significance is the observation that TbRAB5A^{QL} increased LDL and LY uptake in procyclics to levels similar to bloodstream forms, suggesting an additional rate-limiting com-

ponent in this stage. Because the base rate of endocytosis in bloodstream form is one of the highest reported in any system, this restriction may even be a structural limitation. Importantly, these data also separate the functions of TbRAB5A and TbRAB5B as the former is implicated as controlling LDL endocytosis and the latter is not, suggesting that despite colocalization in procyclics these two Rabs have nonidentical roles.

The influence of TbRAB5A on LDL endocytosis illuminates additional aspects of LDL receptor function. Our data confirm earlier binding studies and localization data; the receptor is present on the flagellum and flagellar pocket, and there are two distinct binding site classes (17). We extended these observations by observing a specific increase in surface-binding sites. Most importantly, the ratio of high to low affinity sites was precisely maintained, suggesting that the same molecule indeed gives rise to both sites. Based on this, our recent identification of clathrin-coated vesicles and pits restricted to the flagellar pocket (15) and the location of the LDL-binding sites revealed with fluorescent LDL, we propose that high affinity sites are due to clustering of the receptor in the flagellar pocket, whereas the more abundant low affinity sites are monomeric receptors arrayed on the flagellum.

In conclusion, TbRAB5A and TbRAB5B have distinct roles in *T. brucei,* and active sorting of endocytic cargo is a feature of the trypanosome endosome system suggesting a level of sophistication permitting independent responses to different classes of endocytic cargo. This may include the ability to rapidly recycle VSG for removal of surface immunoglobulin without detrimental effects on endocytosis of other surface components.

REFERENCES

1. Cross, G. A. M. (1990) *Annu. Rev. Genet.* **8,** 83–110
2. Pays, E., Lips, S., Nolan, D., Vandamme, L., and Perez-Morga, D. (2001) *Mol. Biochem. Parasitol.* **114,** 1–16
3. Smith, A. B., Esko, J. D., and Hadjuk, S. L. (1993) *Science* **268,** 284–286
4. Raper, J., Portela, M. P., Lugli, E., Frevert, U., and Tomlinson, S. (2001) *Curr. Opin. Microbiol.* **4,** 402–408
5. Hager, K. M., and Hajduk, S. L. (1997) *Nature* **385,** 823–826
6. O'Beirne, C., Lowry, C. M., and Voorheis, H. P. (1998) *Mol. Biochem. Parasitol.* **911,** 165–193
7. Ferguson, M. A. (2000) *Proc. Natl. Acad. Sci. U. S. A.* **97,** 10673–10675
8. Ilg, T. (2000) *Parasitol. Today* **16,** 489–497
9. Field, H., Farjah, M., Pal, A., Gull, K., and Field, M. C. (1998) *J. Biol. Chem.* **273,** 32102–32110
10. Nolan, D. P., Jackson, D. G., Windle, H. J., Pays, A., Geuskens, M., Michel, A., Voorheis, H. P., and Pays, E. (1997) *J. Biol. Chem.* **272,** 29212–29221
11. Kelley, R. J., Brickman, M. J., and Balber, A. E. (1995) *Mol. Biochem. Parasitol.* **74,** 167–178
12. Nolan, D. P., Geuskens, M., and Pays, E. (1999) *Curr. Biol.* **9,** 1169–1172
13. Denny, P. W., Field, M. C., and Smith, D. F. (2001) *FEBS Lett.* **491,** 148–153
14. Liu, J., Qiao, X., Du, D., and Lee, M. G. (2000) *J. Biol. Chem.* **275,** 12032–12040
15. Morgan, G. W., Allen, C. L., Holinshead, M., Jeffries, T., and Field, M. C. (2001) *J. Cell Sci.* **114,** 2605–2616
16. Coppens, I., Opperdoes, F. R., Courtoy, P. J., and Baudhuin, P. (1987) *J. Protozool.* **34,** 465–473
17. Coppens, I., Baudhuin, P., Opperdoes, F. R., and Courtoy, P. J. (1988) *Proc. Natl. Acad. Sci. U. S. A.* **83,** 6753–6757
18. Salmon, D., Hancq-Quertier, J., Paturiaux-Hanocq, F., Pays, A., Tebabi, P., Nolan, D. P., Michel, A., and Pays, E. (1997) *EMBO J.* **16,** 7272–7278
19. Zerial, M., and McBride, H. (2001) *Nat. Rev. Mol. Cell. Biol.* **2,** 107–117
20. Rybin, V., Ullrich, O., Rubino, M., Alexandrov, K., Simon, I., Seabra, M. C., Goody, R., and Zerial, M. (1996) *Nature* **383,** 266–269
21. Christoforidis, S., Miaczynska, M., Ashman, K., Wilm, M., Zhao, L., Yip, S. C., Waterfield, M. D., Backer, J. M., and Zerial, M. (1999) *Nat. Cell Biol.* **1,** 249–252
22. Segev, N. (2001) *Cell Biol.* **13,** 500–511
23. Stenmark, H., Parton, R. G., Steele-Mortimer, O., Lutcke, A., Gruenberg, J., and Zerial, M. (1994) *EMBO J.* **13,** 1287–1296
24. Singer-Kruger, B., Stenmark, H., Dusterhoft, A., Philippsen, P., Yoo, J. S., Gallwitz, D., and Zerial, M. (1994) *J. Cell Biol.* **125,** 283–298

25. Alvarez-Dominguez, C., and Stahl, P. D. (1999) *J. Biol. Chem.* **274,** 11459–11462
26. Barbieri, M. A., Roberts, R. L., Gumusboga, A., Highfield, H., Alvarez-Dominguez, C., Wells, A., and Stahl, P. D. (2000) *J. Cell Biol.* **151,** 539–550
27. Jeffries, T. R., Morgan, G. W., and Field, M. C. (2001) *J. Cell Sci.* **114,** 2617–2626
28. Field, H., Ali, B. R. S., Sherwin, T., Gull, K., Croft, S. L., and Field, M. C. (1999) *J. Cell Sci.* **112,** 147–156
29. Brun, R., and Schonenberger, M. (1979) *Acta Trop.* **36,** 286–292
30. Bangs, J. D., Brouch, E. M., Ransom, D. M., and Roggy, J. L. (1996) *J. Biol. Chem.* **271,** 18387–18393
31. Medina-Acosta, E., and Cross, G. A. M. (1993) *Mol. Biochem. Parasitol.* **59,** 327–330
32. Laemmli, U. K. (1970) *Nature* **227,** 680–685
33. Foster, R., Hu, K.-Q., Lu, Y., Nolan, K. M., Thissen, J., and Settleman, J. (1996) *Mol. Cell. Biol.* **16,** 2689–2699
34. Pitas, R. E., Innerarity, T. L., Arnold, K. S., and Mahley, R. W. (1979) *Proc. Natl. Acad. Sci. U. S. A.* **76,** 2311–2315
35. Field, H., Blench, I., Croft, S., and Field, M. C. (1996) *Mol. Biochem. Parasitol.* **82,** 67–80
36. Langreth, S. G., and Balber, A. (1975) *J. Protozool.* **22,** 40–53
37. Hajduk, S. L., Hager, K. M., and Esko, J. D. (1994) *Annu. Rev. Microbiol.* **48,** 139–162
38. Coppens, I., and Courtoy, P. J. (1995) *Mol. Biochem. Parasitol.* **73,** 179–187
39. Steverding, D. (2000) *Parasitol. Int.* **48,** 191–198
40. Weise, F., Stierhof, Y. D., Kuhn, C., Wiese, M., and Overath, P. (2000) *J. Cell Sci.* **113,** 4587–4603
41. Sonnichsen, B., De Renzis, S., Nielsen, E., Rietdorf, J., and Zerial, M. (2000) *J. Cell Biol.* **149,** 901–914
42. Burleigh, B. A., Wells, C. W., Clarke M. W., and Gardiner, P. R. (1993) *J. Cell Biol.* **120,** 339–352
43. McDowell, M. A., Ransom, D. M., and Bangs, J. D. (1998) *Biochem. J.* **335,** 681–689
44. Acosta-Serrano, A., Vassella, E., Liniger, M., Kunz-Renggli, C., Brun, R., Roditi, I., and Englund, P. T. (2001) *Proc. Natl. Acad. Sci. U. S. A.* **98,** 1513–1518